# Fiber-optic, cantilever-type acoustic motion velocity hydrophone

G. A. Cranch,[a] G. A. Miller, and C. K. Kirkendall
*Naval Research Laboratory, 4555 Overlook Avenue Southwest, Washington, DC 20375*

(Received 13 July 2011; revised 24 January 2012; accepted 29 April 2012)

The interaction between fluid loaded fiber-optic cantilevers and a low frequency acoustic wave is investigated as the basis for an acoustic vector sensor. The displacements of the prototype cantilevers are measured with an integrated fiber laser strain sensor. A theoretical model predicting the frequency dependent shape of acoustically driven planar and cylindrical fiber-optic cantilevers incorporating effects of fluid viscosity is presented. The model demonstrates good agreement with the measured response of two prototype cantilevers, characterized with a vibrating water column, in the regime of $Re \geq 1$. The performance of each cantilever geometry is also analyzed. Factors affecting the sensor performance such as fluid viscosity, laser mode profile, and support motion are considered. The planar cantilever is shown to experience the largest acoustically induced force and hence the highest acoustic responsivity. However, the cylindrical cantilever exhibits the smoothest response in water, due to the influence of viscous fluid damping, and is capable of two axis particle velocity measurement. These cantilevers are shown to be capable of achieving acoustic resolutions approaching the lowest sea-state ocean noise. [http://dx.doi.org/10.1121/1.4725764]

PACS number(s): 43.30.Yj, 43.38.Ar, 43.38.Zp, 43.58.Wc [DAB] Pages: 103–114

## I. INTRODUCTION

The benefits of characterizing an acoustic field by measuring particle motion, instead of local changes in ambient pressure, have long been known. Measurement of the particle motion in terms of displacement, velocity, or acceleration reveal information on the field direction as well as amplitude. Simultaneous measurement of the local pressure, $p$, and particle velocity, $\dot{u}$, in a plane wave also yields the acoustic intensity through the relationship, $I = \langle real(p) real(\dot{\mathbf{u}}) \rangle_T$, where $\langle \rangle_T$ denotes time average. When it is of interest to detect and locate sources of acoustic radiation through the use of coherently beamformed arrays, particle motion sensors provide further benefits due to their inherent directionality. An array of three-axis directional sensors achieves equal array gain to an array of scalar hydrophones with twice the length.[1] Furthermore, the left-right ambiguity arising from the symmetry of scalar sensor line arrays is overcome with arrays of directional sensors.[2]

Most sensors designed to respond to acoustic particle motion are based on some form of simple harmonic mechanical oscillator that is driven by the acoustically induced motion. The operating bandwidth of the sensor is determined by the fundamental resonant frequency of the oscillator. Assuming the sensor responds linearly to the relative displacement between the inertial mass and its case, then operation below the fundamental resonance will result in a response to acceleration independent of frequency (i.e., an accelerometer). Operation above the fundamental resonance results in a response to displacement independent of frequency. One such sensor, known as the moving coil geophone, that operates above the fundamental resonance responds to the rate of change of the sensor casing and thus responds to velocity independent of frequency.

For measuring low frequency (i.e., $<10$ kHz) acoustic fields in the ocean, a frequency independent or smooth response to particle velocity is highly desirable. In a planar wave field, the acoustic impedance relating the ratio of the pressure to particle velocity is given by the product of fluid density and sound speed, $\rho_{fl} c_{fl}$. Thus, the ambient velocity noise field is proportional to the pressure field. This is beneficial since the spectral density of the ambient acoustic pressure noise exhibits an approximately, $1/f^n$ dependence, which is a similar dependence to the internal electronic noise spectrum in many sensors, particularly at low frequencies. Consequently, when the limiting noise source is ambient acoustic, the acoustic resolution is not diminished for deceasing frequency with a true velocity sensor. The interest in developing low frequency vector sensors is apparent from the number of reported devices. For example, devices based on moving coil,[3,4] piezoelectric,[5] resistive heating,[6] and magnetostrictive[7] mechanisms have been demonstrated. Also, several fiber-optic devices have been demonstrated based on flexural disk[8,9] and bending beam[10] accelerometers, and pressure gradient hydrophones.[11] However, achieving high acoustic sensitivity over a large bandwidth from a small sensor remains a challenge.

In the current work, a new concept for a particle motion sensor is investigated. The sensor is based on the acoustically driven motion of a fluid loaded fiber-optic cantilever. Both cylindrical and planar cantilevers are investigated (some results for the planar cantilever have been previously published in Ref. 12). Although, essentially behaving as a driven mechanical oscillator, the implementation of the sensing mechanism results in unique behavior that is evidently well suited to measurement of low frequency acoustic fields. The current work has a number of novel aspects: (a) the dominant damping mechanism for both planar and cylindrical fiber-optic cantilever geometries is identified and incorporated into a theoretical

[a]Author to whom correspondence should be addressed. Electronic mail: geoff.cranch@nrl.navy.mil

model, (b) expressions for the acoustically induced driving force are derived for both cylindrical and planar cantilevers and their validity is demonstrated with finite element modeling and experimental measurements in the regimes of low to moderate fluid viscosity, (c) the model is used to determine important design parameters for an acoustic sensor, and (d) compelling evidence is presented to suggest that acoustically insonified optical fiber in a fluid exhibits a response strongly affected by the particle motion, which in certain circumstances may dominate the response due to hydrostatic pressure changes. This last point is significant, since early research on the acoustic transduction mechanism of optical fiber was concerned primarily with its response to hydrostatic pressure changes[13–15] and generally neglected inertial and viscous effects which are shown here to be very significant.

The deflections of the cantilever are measured with a fiber laser sensor.[16] This fiber optic sensor provides very high sensitivity to axial strain induced in the core through flexure of the optical fiber, necessary for acoustic measurements. Along with the established benefits of fiber optic sensors for undersea acoustic measurements such as excellent long term reliability, low weight, and immunity to electromagnetic interference, an acoustic vector sensor based on the present concept has many other favorable attributes: (a) it can be made very small and lightweight since the fiber constitutes both the mechanical oscillator and the sensor, (b) a single multicore fiber can potentially measure two vector components of the acoustic field, and (c) a smooth response to particle velocity can be achieved due to significant viscous fluid damping arising from low Reynolds number flow around a small cantilever.

Although fiber-optic flow sensors that respond to the viscous fluid force have been demonstrated based on twin-core optical fiber,[17] only one previous effort to develop an acoustic sensor of this type has been reported. Josserand *et al.*[18] characterized the acoustic response of a planar PVF2 cantilever. A simple model was presented to describe the cantilever motion but the exact expression for the acoustic driving force was not clear and viscous forces, which are shown to be significant in the current work, were neglected. Although the results demonstrated were encouraging, the size of the device resulted in a strongly peaked resonant response to particle velocity at low frequencies, which is generally undesirable.

This article is arranged as follows. An analytical model of the response of the fluid loaded cantilever is described in Sec. II. Expressions for the acoustic driving force are presented and results from the analytical model are compared with a finite-element model of the acoustic-structure interaction. The characterization of the cantilevers in air and water is described in Sec. III and the measured responses are compared with results from the analytical models. A discussion is then given on the dependence of the acoustic response on the size and geometry of the cantilever and the predicted acoustic resolution in Sec. IV. Finally the conclusions are summarized in Sec. V.

## II. THEORY

The geometries of the planar and cylindrical cantilevers are illustrated in Figs. 1(a) and 1(b), respectively. The planar

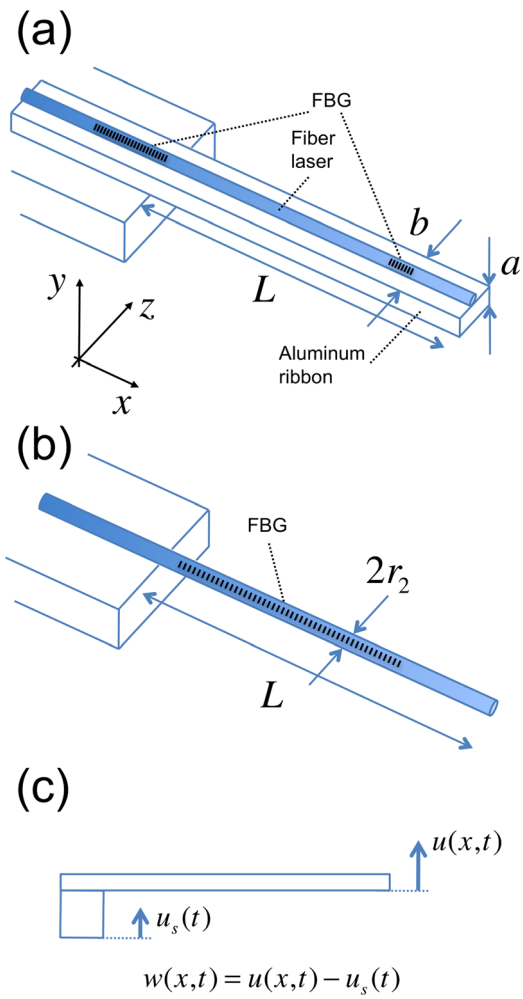


FIG. 1. (Color online) Cantilever geometries (a) planar cantilever comprising a silica optical fiber with an acrylate coating bonded to an aluminum ribbon, (b) cylindrical cantilever comprising a silica optical fiber with an acrylate coating only, and (c) displacements of cantilever and support.

cantilever consists of a thin ribbon with an optical fiber attached to its upper surface. The cylindrical cantilever consists of a single optical fiber. Both cantilevers are rigidly fixed to an aluminum support. In the subsequent analysis the following assumptions are made.

(a) The cross section of the cantilever is uniform along its length.
(b) The cantilever length greatly exceeds its width or diameter (i.e., it is long and slender).
(c) The beam is isotropic in the x-direction.
(d) The smallest dimension of the beam greatly exceeds the amplitude of the vibration.
(e) The shortest wavelength of the acoustic excitation greatly exceeds the largest dimension of the beam.
(f) The surrounding fluid is unbounded within a region much larger than the largest cross-sectional dimension of the cantilever.

Furthermore, the laser is assumed to respond only to flexural vibration modes, thus transverse modes (in the z-direction) are neglected.

Of particular interest is the effect of viscous fluid damping on the response of the cantilever which becomes significant at

low Reynolds number. The Reynolds number for the acoustically induced flow can be defined in terms of the dominant length scale of the cantilever as[19]

$$Re = \frac{\rho_{fl}\omega b^2}{4\eta}. \tag{1}$$

Here $\rho_{fl}$ is the fluid density, $\omega$ is the acoustic (angular) frequency, $\eta$ is the dynamic viscosity of the fluid, and $b$ is the width of the planar cantilever or outer diameter of the cylindrical cantilever. The relative importance of viscous effects on the sensor behavior will therefore depend on operating frequency due to the dependence of $Re$ on $\omega$.

### A. Beam theory

Many studies on the behavior of fluid loaded beams have been previously reported.[20–25] Although the later models incorporate the effect of acoustic radiation losses[24,25] all of these analyses assume the fluid is inviscid. Furthermore, radiation losses in the current sensor are expected to be small due to the acoustic wavelength greatly exceeding the cantilever dimensions. A more recent model incorporating viscous losses was reported by Sader[19] who analyzed the thermally driven response of a micro-cantilever in a viscous fluid. This model was later experimentally verified.[26] The Sader model is used as the basis for understanding the behavior of the fiber-optic cantilever. This model is extended by considering the cantilever motion when driven by acoustically induced fluid motion and support motion.

The deflections of the cantilever when submerged in a viscous fluid are described by the beam equation

$$EI\frac{\partial^4 u(x,t)}{\partial x^4} + \mu\frac{\partial^2 u(x,t)}{\partial t^2} = f_h(x,t), \tag{2}$$

where $EI$ is the beam stiffness, $u(x, t)$ is the absolute displacement of the beam in the y-direction, $\mu$ is the mass per unit length of the cantilever, and $f_h(x, t)$ is the hydrodynamic force. This equation represents the balance of forces on the cantilever when brought into motion. The sum of the restoring force due to the beam stiffness and the inertial force of the cantilever is equal to the force exerted by the fluid. This force due to the fluid is known as the hydrodynamic force and incorporates the effect of the additional inertia of the fluid and its viscosity for unsteady (or oscillatory) boundary flow. Equation (2) can be solved using the boundary conditions for a beam of length, $L$, clamped at one end,

$$u(0,t) = u_s(t), \quad \frac{\partial u(0,t)}{\partial x} = 0 \tag{3}$$

and

$$\frac{\partial^2 u(L,t)}{\partial^2 x} = 0, \quad \frac{\partial^3 u(L,t)}{\partial^3 x} = 0, \tag{4}$$

where $u_s(x, t)$ is the displacement of the support. It is convenient to transform Eq. (2) into the frequency domain to analyze steady-state behavior such that

$$EI\frac{\partial^4 U(x|\omega)}{\partial x^4} + \mu\frac{\partial^2 U(x|\omega)}{\partial t^2} = F_h(x|\omega), \tag{5}$$

where $U(x|\omega)$ represents the Fourier transform of $u(x, t)$. Assuming harmonic motion of the form, $u(x,t) = u_0(x)\exp(iwt)$, then Eq. (5) becomes

$$EI\frac{\partial^4 U(x|\omega)}{\partial x^4} - \mu\omega^2 U(x|\omega) = F_h(x|\omega). \tag{6}$$

The hydrodymanic force, presented by Rosenhead[27] and also used by Sader,[19] is given by

$$F_h(x|\omega) = \mu'\Gamma(\omega)\omega^2 U(x|\omega), \tag{7}$$

where $\mu'$ is the added mass per unit length due to the fluid and $\Gamma(\omega)$ is the geometry dependent hydrodynamic function and in general is complex. The term $\mu'\Gamma(\omega)$ is known as the "virtual" mass of the fluid.

Consider first the case where the cantilever is brought into motion by applying a displacement to the support, as illustrated in Fig. 1(c). The device will measure the relative displacement between the support and the beam (i.e., the beam shape), which is given by $W(x|\omega) = U(x|\omega) - U_s(\omega)$. Substituting Eq. (7) into Eq. (6) and expressing in terms of the beam shape, $W(x|\omega)$, yields

$$EI\frac{\partial^4 W(x|\omega)}{\partial x^4} - (\mu + \mu'\Gamma(\omega))\omega^2 W(x|\omega) = F_{dr-SM}(\omega) \tag{8}$$

where the general form of the driving force due to support motion, $F_{dr-SM}(\omega)$, is given by

$$F_{dr-SM}(\omega) = (\mu + \mu'\Gamma(\omega))\omega^2 U_s(\omega). \tag{9}$$

The hydrodynamic force has added the virtual mass term to the inertial term on the left-hand side of Eq. (8). This acts to shift the resonant frequency and adds damping due to the fluid viscosity. The virtual mass is also added to the driving force causing it to be enhanced, compared with its magnitude in a vacuum (i.e., where $\mu' = 0$). Equation (8) represents the equation of motion for a fluid loaded cantilever subject to support motion.

An alternative means of actuating the cantilever is by fluid motion. This can be implemented by exciting an acoustic wave in the fluid and corresponds to the relevant transduction mechanism for the present sensor. In this case $U_s = 0$ (i.e., the support motion is zero) and an additional term, $F_{dr-FM}(\omega)$, must be added to the right-hand side of Eq. (6) to account for this fluid motion. The equation of motion in this case is given by

$$EI\frac{\partial^4 W(x|\omega)}{\partial x^4} - (\mu + \mu'\Gamma(\omega))\omega^2 W(x|\omega) = F_{dr-FM}(\omega). \tag{10}$$

The general form of the driving force due to fluid motion is

$$F_{dr-FM}(\omega) = \mu'\Gamma(\omega)\omega^2 U_{fl}(\omega), \tag{11}$$

where $U_{fl}(\omega)$ is the displacement of the fluid in the absence of the cantilever. Typically, $\mu'\Gamma(\omega)$ is much larger than $\mu$ and therefore the response under actuation by support motion, according to Eq. (9), will be similar to that under fluid motion when $U_s = U_{fl}$. Equations (8) and (10) are similar in form to Eq. (11) derived in Ref. 28 for a piezoelectrically actuated microcantilever used in atomic force microscopes.

The driving force from a plane acoustic wave, which creates the pressure gradient parallel to the motion of the cantilever, can be derived from this result. A small volume element of fluid in an acoustic field experiences a force per unit length given by $d\vec{f}(x,y,z) = -dA \cdot \nabla p(x,y,z)$, where $p$ is the acoustic pressure, $\nabla = \partial/\partial x \cdot \vec{i} + \partial/\partial y \cdot \vec{j} + \partial/\partial z \cdot \vec{k}$, and $dA$ is the area across which the force acts. According to the linear inviscid force equation for small amplitude acoustic processes,[29] the pressure gradient is also proportional to the fluid acceleration

$$\rho_{fl}\frac{\partial \dot{u}_{fl}}{\partial t} = -\nabla p. \tag{12}$$

A plane wave traveling in the y-direction takes the form, $p = p_0 \exp(i(\omega t - ky))$, where $k$ is the acoustic wavenumber $(k = \omega/c_{fl})$ and $c_{fl}$ is the sound speed in the fluid. Assuming the acoustic wavelength is much larger than the dimensions of the cantilever, then using Eqs. (11), (12) and the relation $df_y = -A_e \cdot \partial p/\partial y$ yields the Fourier transform of the force due to the fluid motion in terms of acoustic pressure

$$F_{dr-aco}(\omega) = -iA_e\Gamma(\omega)\cdot\frac{\omega}{c_{fl}}p_y. \tag{13}$$

$A_e$ corresponds to the effective area over which to calculate the pressure gradient and is given by $\mu'/\rho_{fl}$.

### 1. Effect of geometry

Thus far the analysis has not considered the geometry of the cantilever. This establishes the effective mass of the fluid and the form of the hydrodynamic function, $\Gamma(\omega)$. The effective mass of the fluid has been derived by Chu for the case of the planar cantilever and is given by[20,30]

$$\mu'_{pl} = \rho_{fl}\pi b^2/4. \tag{14}$$

The effective mass of the fluid is equivalent to the mass of a fluid cylinder with a diameter equal to the width of the cantilever, $b$. The expression for the cylindrical cantilever is the same as the planar cantilever with $b$ replaced with the outer diameter of the cylindrical cantilever, $2r_2$. This result suggests that a cylindrical region of fluid surrounding the cantilever is closely coupled to it and strongly influences its motion. This is also the region where the fluid motion is strongly perturbed by the cantilever motion. The expression (14) is widely used to predict the change in resonance frequency of a beam submerged in an inviscid fluid.

The hydrodymanic function incorporates the effect on the cantilever motion of the fluid viscosity and depends on the geometry of the cantilever. An analytical solution exists for the cylindrical cantilever and is given by

$$\Gamma_{circ}(\omega) = 1 + \frac{4iK_1(-i\sqrt{iRe})}{\sqrt{iRe}K_0(-i\sqrt{iRe})}, \tag{15}$$

where $K_n$ are modified Bessel functions of the second kind. An analytical solution for the planar cantilever does not exist, however, Sader derived an approximate solution by noting that the hydrodynamic function for the cylindrical and planar cantilever possess the same asymptotic form in the limits $Re \to 0$ and $Re \to \infty$. In the simulations that follow, this approximate expression is used for the hydrodynamic function for the planar cantilever. However, it should be noted that this approximate expression deviates from the exact expression for the cylindrical cantilever by less than 12% over the range $10^{-4} < Re < 10^2$. Therefore, $\Gamma$ is similar for both cantilever geometries. The real and imaginary parts of $\Gamma(\omega)$ are plotted in Fig. 2. For large $Re$, the imaginary part is negligible and $\Gamma \sim 1$ corresponding to an inviscid fluid. When $Re \ll 1$ the imaginary part is much larger than the real part, which has interesting consequences for the driving force. The sensor behavior can be separated into three different operating regimes depending on the Reynolds number, illustrated in Fig. 2. These will now be examined in more detail.

### 2. Driving force—high Re regime

This regime occurs, according to Eq. (1), at high frequencies or when the cantilever dimensions increase, and represents small or negligible viscous effects. It is obtained when the prototype cantilevers described here are operated in air. In water, this regime is obtained when the cantilever cross section is larger than a few millimeters and is experienced by the planar cantilever described here. When viscous damping is small, the frequency response of the cantilever exhibits sharp peaks at each resonance and as a sensor is generally not suitable for operation above the fundamental resonance. If the cantilever were driven by an acoustic wave propagating in air, the driving force generated by air particle

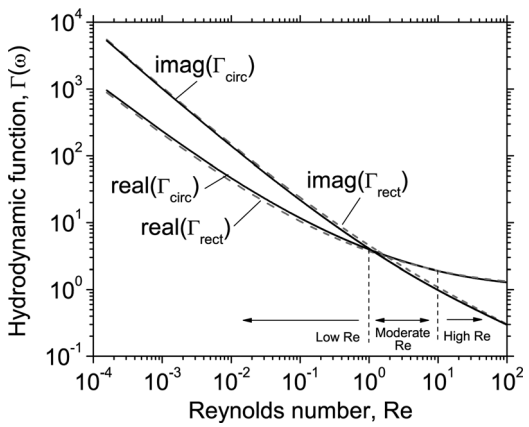


FIG. 2. Real and imaginary parts of the hydrodynamic function for the cylindrical and planar cantilever (solid line—cylindrical cantilever, dashed line—planar cantilever).

motion, according to Eq. (11), will be very small due to a small value of $\mu'$ yielding a very low response.

An alternative configuration for an acoustic sensor operating in a liquid is to place the cantilever in a sealed neutrally buoyant enclosure, which is submerged in the liquid. An acoustic wave propagating in the liquid induces motion of the support through the enclosure. The cantilever motion will be described by Eq. (8) and the force is given by

$$F_{dr-SM}(\omega)|_{high-Re} \simeq \mu\omega^2 U_s(\omega). \tag{16}$$

The driving force is dependent on the mass of the beam, $\mu$. Such a configuration is similar to that demonstrated in Ref. 10. For a planar cantilever, this force is somewhat smaller than the force experienced by the cantilever when submerged in a liquid and driven directly by the acoustic wave. In this case, the force is dependent on the effective mass of the surrounding water. This implies an added benefit of a directly driven cantilever.

#### 3. Driving force—moderate Re regime

When $Re$ is less than $\sim$10 the real part of $\Gamma(\omega)$ begins to increase. However, the imaginary part increases more rapidly and becomes equal to the real part when $Re \sim 1$. In this regime, viscous damping is more significant but the driving force is predominantly due to fluid inertia. This regime is experienced by the cylindrical cantilever described here in water. The driving force due to fluid motion is given by Eq. (11) and can be approximated to

$$F_{dr-FM}(\omega)|_{mod-Re} \simeq \mu' real(\Gamma(\omega)) \cdot \omega^2 U_{fl}(\omega). \tag{17}$$

This force is in phase with the acceleration of the cantilever and is thus related to the acceleration of the fluid driven by the pressure gradient across the cantilever (i.e., parallel to its motion). The Fourier transform of the force due to the fluid motion in terms of acoustic pressure is

$$F_{dr-aco}(\omega)|_{mod-Re} \simeq -iA_e\, real(\Gamma(\omega)) \cdot \frac{\omega}{c_{fl}} p_y. \tag{18}$$

In this regime, $\Gamma$ takes a value between 1 and 3. The inviscid form of Eq. (17) [i.e., when $\Gamma(\omega) = 1$] is in agreement with an equivalent expression for an acoustically driven cylinder derived in Ref. 31.

#### 4. Driving force—low Re regime

When $Re$ is less than 1, then $real(\Gamma(\omega)) \ll imag(\Gamma(\omega))$. The driving force due to fluid motion is given by

$$F_{dr-FM}(\omega)|_{low-Re} \simeq \mu' imag(\Gamma(\omega)) \cdot \omega^2 U_{fl}(\omega). \tag{19}$$

The driving force is now dominated by the imaginary part of $\Gamma(\omega)$ and is in phase with the velocity of the cantilever. The cantilever motion in this regime is driven predominantly by the fluid viscosity. Referring to Fig. 2, the imaginary part of $\Gamma(\omega)$ increases rapidly with decreasing $Re$, approaching $\sim$1000 for $Re \sim 10^{-3}$. The magnitude of this force is very large compared with the other two regimes and therefore represents an interesting operating regime for a fluid motion sensor.

The Fourier transform of the force in terms of acoustic pressure is given by

$$F_{dr-aco}(\omega)|_{low-Re} \simeq -iA_e imag(\Gamma(\omega)) \cdot \frac{\omega}{c_{fl}} p_y. \tag{20}$$

#### 5. Calculating the beam shape

The normalized beam shape is given by the analytical solution to the equation of motion (6), which was derived by Sader using a Green's function method and is given in Appendix A of Ref. 19. This solution is used along with the driving forces derived above to determine the beam deflections.

### B. Comparison of analytical and finite-element models

To confirm the validity of the acoustically induced force derived above, the inviscid form of the analytical model [i.e., Eqs. (10) and (11) with $\Gamma = 1$] is compared with a finite element model for each cantilever. The finite-element (FE) model is developed in COMSOL MULTIPHYSICS as a three dimensional acoustic-structure interaction, details of which are given in Appendix A. For both models the beam shape is derived as a function of drive frequency. This is used to determine the flexure strain induced in the core of the optical fiber, $\Delta\epsilon(x, t)$. The shift in laser frequency, $\Delta\nu_l$, is then calculated using[32]

$$\frac{\Delta\nu_l}{\nu_l} = (0.78)\frac{1}{L_c}\int_{x_1}^{x_2} \Delta\varepsilon(x,t)\hat{A}\,(x)dx, \tag{21}$$

where $\hat{A}\,(x)$ is the spatial distribution of the laser mode intensity and $L_c$ is the effective cavity length.

The results from the two models for each cantilever geometry are shown in Fig. 3 as solid lines for the analytical model and symbols for the FE model. Details on calculating the mechanical properties of the cantilevers for the analytical model are given in Appendix B. For each case the simulation is run for fluid densities of 10 and 1000 kg/m$^3$. In both cases the agreement is excellent. The close agreement at low frequencies confirm the validity of the expressions for the driving force for an inviscid fluid. The change in fluid density affects the mass loading, shifting the resonant frequencies.

## III. EXPERIMENT

In the following experimental section, the response of the cantilevers is characterized and compared to the theoretical response according to the analytical model presented in Sec. II in the operating regimes of moderate and high $Re$.

The planar cantilever is 40 mm in length and consists of an aluminum ribbon with cross-section 3 mm $\times$ 50 $\mu$m. It comprises a fiber laser adhered to an aluminum ribbon using a thin layer of rapid cure epoxy. The fiber laser comprises

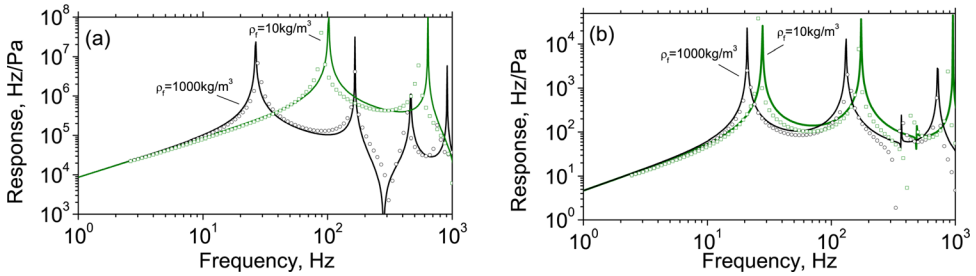


FIG. 3. (Color online) Comparison of analytical model (solid lines) with finite-element acoustic-structure interaction model (symbols) for (a) planar cantilever and (b) cylindrical cantilever. Both models are inviscid. For this simulation, the flexural strain is integrated over the length of the cantilever (i.e., the laser mode function is unity).

two fiber Bragg gratings separated by 20 mm written into an erbium doped fiber. Only the cavity of the laser (~20 mm in length) is adhered to the ribbon, which is positioned at the base of the cantilever, to avoid distortion of the Bragg gratings. The prototype is shown in Fig. 4. The fiber comprises a 125 $\mu$m silica cladding with a 138 $\mu$m thick acrylate jacket. The core is approximately 200 $\mu$m from the neutral surface of the cantilever.

The cylindrical cantilever is 55 mm in length and consists of a 125 $\mu$m diameter erbium doped silica fiber with a 62.5 $\mu$m thick acrylate coating. A fiber laser consisting of a 50 mm Bragg grating with a centrally located $\pi$ phase-shift is formed in the core of the optical fiber. This type of laser is known as a distributed feedback (DFB) laser and exhibits an optical mode tightly confined about the phase-shift. The Bragg grating strength is characterized by its coupling coefficient, $q$, which is $\sim 180\,\mathrm{m}^{-1}$. The phase-shift defines the center of the laser mode and is located close to the center of the cantilever.

The lasers are pumped with 100 mW of 980 nm optical radiation from a laser diode and emit a single optical frequency around 1550 nm. The frequency shifts of the fiber laser are measured using an unbalanced fiber-optic interferometer.[16] The cantilever is characterized in air by applying a known acceleration to the support. The output frequency shift of the laser as a function of frequency is calibrated relative to a reference piezoelectric accelerometer, also attached to the support. Acoustic characterization of the cantilevers is carried out using a vibrating water column, described in Appendix C, which enables acoustic calibration from approximately 10 Hz to 1 kHz. Inertial excitation is achieved with a shaker table (Bruel & Kjaer 4808).

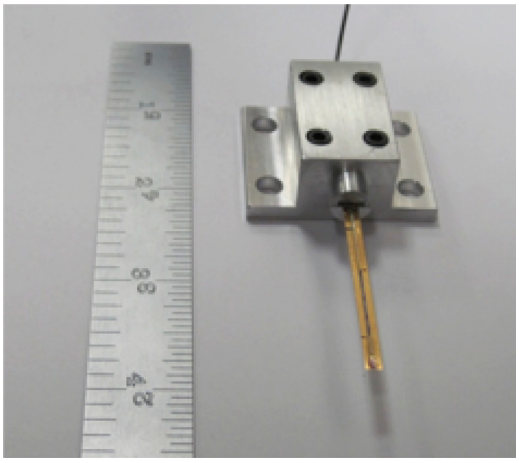

FIG. 4. (Color online) Prototype planar cantilever.

According to Eq. (1), for a frequency of 100 Hz and assuming the fluid to be water, $Re \sim 1410$ for the planar cantilever and $Re \sim 10$ for the cylindrical cantilever. Therefore, viscous damping is expected to be much more significant for the cylindrical cantilever. Material parameters used in the following theoretical calculations are given in Table I.

### A. Planar cantilever

The acceleration response measured in air (in units of GHz/g) for the planar cantilever is shown in Fig. 5(a). The response exhibits a fundamental resonance at 121 Hz with an overtone at 751 Hz. The predicted response according to the analytical model is also overlaid. It is assumed that the coupling of the laser cavity with the aluminum ribbon occurs over ~0.5 of its total cavity length, which is consistent with the bonded region of the laser to the ribbon. Good agreement between the theoretical and measured response is obtained at frequencies away from resonant peaks. An appreciable amount of structural damping present in the prototype sensor

TABLE I. Definition of terms.

| Parameter | Definition | Value |
|---|---|---|
| *Fluid properties* | | |
| $\rho_{fl}$ | Density | $997\,\mathrm{kg\,m^{-3}}$ |
| $c_{fl}$ | Sound speed | $1482\,\mathrm{m\,s^{-1}}$ |
| $u$ | Particle displacement | |
| $\dot{u}$ | Particle velocity | |
| $\ddot{u}$ | Particle acceleration | |
| $\eta$ | Fluid viscosity (water) | $8.9 \times 10^{-4}\,\mathrm{Pa\,s}$ |
| $p$ | Acoustic pressure | |
| *Fiber properties* | | |
| $\rho_f$ | Density | $2200\,\mathrm{kg\,m^{-3}}$ |
| $E$ | Youngs modulus | 70 GPa |
| $r_2$ | Coating radius | |
| *Ribbon properties* | *(for planar cantilever)* | |
| $\rho_c$ | Density | $2700\,\mathrm{kg\,m^{-3}}$ |
| $L$ | Length | |
| $b$ | Width | 3 mm |
| $a$ | Thickness | 50 $\mu$m |
| *Miscellaneous* | | |
| $I$ | Second moment of area | |
| $\nu_l$ | Laser frequency | |
| $\Delta\epsilon$ | Local strain | |
| $A(x)$ | Laser mode shape | |
| $q$ | Grating coupling coefficient | |
| $u(x, t)$, $U(x\|\omega)$ | Absolute beam displacement | |
| $u_s(t)$, $U_s(\omega)$ | Support displacement | |
| $w(x, t)$, $W(x\|\omega)$ | Beam shape | |
| $f(x, t)$, $F(x\|\omega)$ | Driving force | |

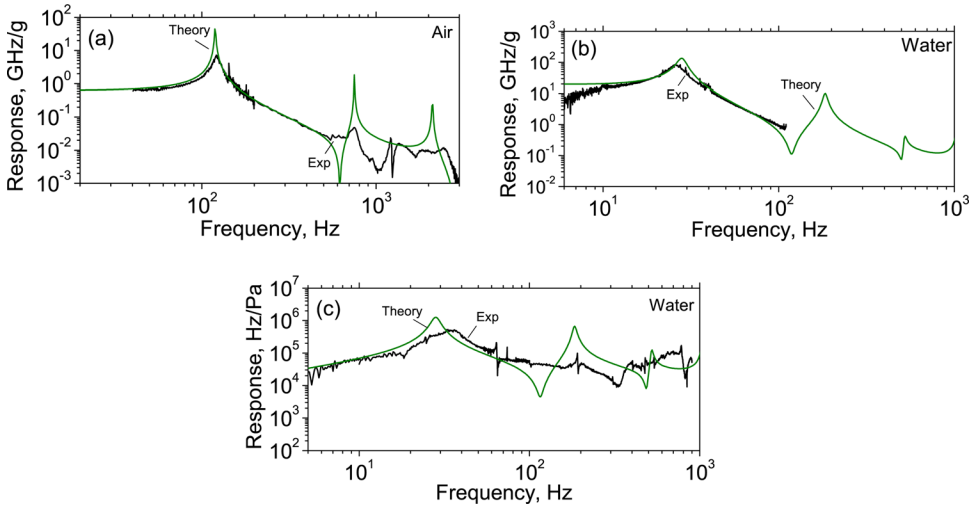


FIG. 5. (Color online) Planar cantilever: (a) acceleration response in air, (b) acceleration response in water, and (c) acoustic response in water. Theoretical responses according to the analytical model are also shown.

is evident from the reduced amplitude of the resonant peaks. This structural damping is not accounted for in the analytical model, which incorporates only viscous fluid damping. In air, viscous damping is small, and results in a large deviation in the theoretical and measured response close to the mechanical resonances. This is not of concern in the present work due to our interest in the effects of viscous fluid damping. The theoretical model also deviates significantly above ~1 kHz due to physical imperfections in the cantilever, which distort the beam shape above this frequency.

The acceleration response of the planar cantilever in water is shown in Fig. 5(b). This is obtained by submerging the cantilever into a water reservoir and applying an acceleration to its support using a suspended shaker table. A reference accelerometer, attached to the cantilever support, records the support acceleration. When submerged, the fundamental resonance is shifted down to 26 Hz, due to the fluid loading. The fluid also adds additional viscous damping, reducing the amplitude of the fundamental resonance slightly. The theoretical response, derived using Eq. (9), is in good agreement with the measured response up to 70 Hz, above which the presence of structural damping in the composite cantilever causes deviation between the measured and theoretical response.

The measured and theoretical acoustic response in water are shown in Fig. 5(c). The theoretical response is in close agreement with the measured response at low frequencies, confirming the validity of the driving force given by Eq. (11) in the regime of high *Re*. The presence of structural damping in the composite cantilever causes deviation between the measured and theoretical response close to the resonances. However, the deviation is much smaller than for the in-air case as the viscous fluid damping now becomes more significant. The dramatic drop-out in the theoretical response at 108 Hz is due to the spatial overlap of the laser mode shape and the flexural strain induced by the beam shape. The integral of the product of these two equates to zero at a frequency close to 108 Hz causing this drop-out. This drop-out is less dramatic in the measured data due to physical imperfections in the cantilever, which distort the beam shape at frequencies above ~70 Hz.

### B. Cylindrical cantilever

The cylindrical cantilever consists of an optical fiber with a centrally located core. One would not expect to observe bending induced flexural strain in the core due to its symmetry about the neutral axis. However, the response of the cylindrical cantilever in air measured as a function of rotation indicates the presence of a small offset error causing the laser to respond to flexural motion. This is measured by recording the response of the cylindrical cantilever to acceleration in air as it is rotated in its housing. The normalized response measured at a frequency close to the fundamental resonance as a function of rotation is shown in Fig. 6(a). The measured and theoretical responses in air are shown in Fig. 6(b) when the fiber is rotated to a position of maximum response. The theoretical response is scaled to the measured response indicating a core offset of 216 nm. The response exhibits a fundamental resonance at 23 Hz with an overtone at 144 Hz. Good agreement is obtained up to the fourth modal resonance at 785 Hz. Above this frequency, vibration of the supporting structure distorts the response of the cantilever. A small deviation of the measured resonant amplitudes from the theory is observed, which may be caused by structural damping due to the acrylate coating or the clamp.

The measured and theoretical response to support motion in water is shown in Fig. 6(c). The resonant peaks are now dramatically damped due to the fluid viscosity and reduced in frequency to 10 and 83 Hz for the fundamental and first overtone, respectively. The theoretical response is in very good agreement with the measured response. The close agreement between the measurement and theory up to ~550 Hz arises from the improved uniformity of the cylindrical cantilever along its length, which is essentially free from structural defects compared with the planar cantilever.

The measured and theoretical acoustic response are shown in Fig. 6(d). Very close agreement is observed between the theoretical and measured response confirming the validity of the driving force in the regime of moderate *Re* and the predicted level of fluid damping. Damping due to the fluid viscosity flattens the response to within ±5 dB over the range 10 to 600 Hz. Finally, the directional dependence of the acoustic response in water is also shown in Fig. 6(a).

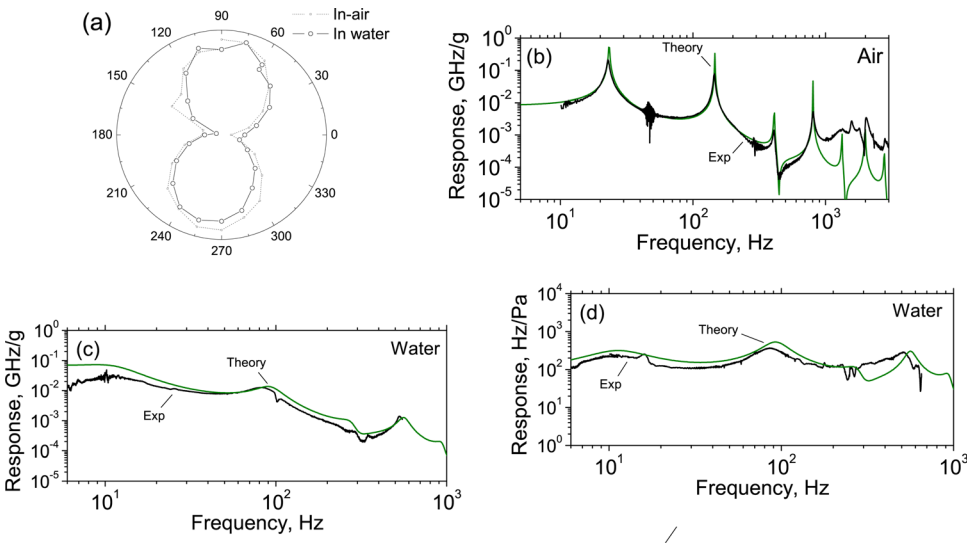


FIG. 6. (Color online) Cylindrical cantilever: (a) directional response, (b) acceleration response in air, (c) acceleration response in water, and (d) acoustic response in water. Theoretical responses, according to the analytical model, are also shown.

This is measured by recording the cantilever response at a frequency close to its fundamental resonance while rotating the cylindrical cantilever in its housing when submerged in the vibrating water column. The directional response in the fluid closely matches the measured directional response in air.

Although some deviations are evident between the theoretical model and the measured responses, particularly at higher frequencies, the overall agreement is very good, confirming the validity of the theoretical approach in the regimes of high and moderate $Re$ (i.e., $Re \geq 1$). Future improvements in mechanical design of the traducers will reduce structural damping and suppress structural resonances associated the cantilever support.

## IV. ANALYSIS

The design considerations for developing an acoustic sensor are to minimize oscillation in the amplitude of the acoustic response over the operating bandwidth and to devise a sensor configuration with the potential for achieving high repeatability of the acoustic response between sensors. Fluid viscosity can be utilized to provide critical damping of the mechanical oscillator to suppress resonant oscillation amplitude and hence smooth the acoustic response. Internal damping mechanisms such as friction at interfaces and support damping must be minimized in order to achieve high fabrication consistency. The effects of the fluid properties and laser mode intensity profile on the sensor response are now considered.

### A. Dependence of response on fluid viscosity

Optimization of the Reynolds number is important for achieving a smooth frequency response. For each cantilever the response is calculated for three different values of $\eta$ using the model presented in Sec. II. The results for the planar cantilever for values of $\eta = 8.9 \times 10^{-4}$, 0.985, and 100 Pa s are shown in Fig. 7. These correspond to $Re$ equal to 1585, 1.4, and 0.01, respectively, calculated at 100 Hz. The first value corresponds to water where the viscous losses are relatively small resulting in multiple peaks appearing in the response due to underdamping. The phase response exhibits abrupt changes at each resonance. Increasing $\eta$ to 0.985 Pa s results in a smooth amplitude and phase response. In this regime, resonant oscillation is entirely suppressed producing a smooth frequency response. This is very close to critical damping and is a suitable operating regime for a sensor. For $\eta = 100$ Pa s the response becomes smoother but steeper, reducing the response at higher frequencies. As $Re$ falls below 1, the driving force becomes dominated by the imaginary part of the hydrodynamic function, $\Gamma(\omega)$, resulting in an increasing response with decreasing frequency. In this regime the cantilever is being driven by the viscosity of the fluid rather than the fluid acceleration.

The corresponding simulation for the cylindrical cantilever is shown in Fig. 8. Here, the response is calculated for $\eta = 8.9 \times 10^{-4}$, $1.65 \times 10^{-2}$, and 0.985 Pa s. These correspond to $Re$ equal to 11, 0.6, and 0.01, respectively, at

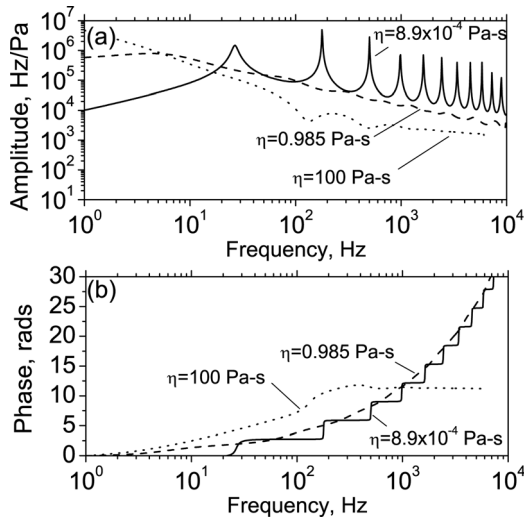


FIG. 7. Dependence of planar cantilever response on fluid viscosity: (a) amplitude and (b) phase. In this simulation the geometry of the cantilever is the same as the prototype cantilever described in Sec. III. $Re$ is varied by changing the viscosity of the surrounding fluid. The laser mode shape is unity over the length of the cantilever.

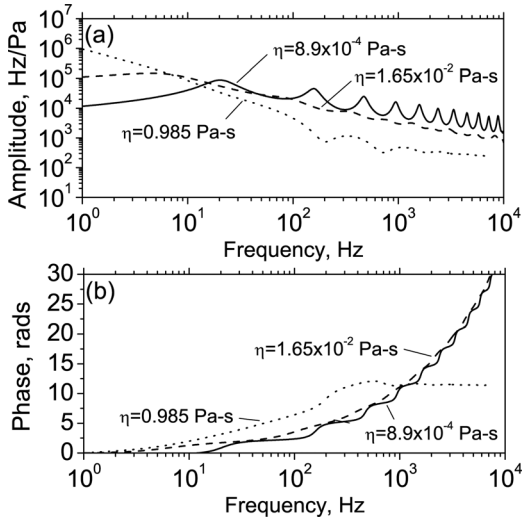


FIG. 8. Dependence of cylindrical cantilever response on fluid viscosity: (a) amplitude and (b) phase. In this simulation the dimensions of the fiber are the same as the prototype cantilever described in Sec. III, however, the length is made equal to the planar cantilever (4 cm) and the core is assumed to be 45 $\mu$m from the center of the optical fiber. The mode shape is unity over the length of the cantilever.

100 Hz. Critical damping is achieved for $Re \sim 0.6$ at 100 Hz yielding a smooth amplitude and phase response. Overdamping is observed for the case of $Re = 0.01$. Similar behavior to the planar cantilever is observed as $Re$ falls below 1.

The similarity in the behavior of the two cantilever geometries for equivalent $Re$ is not unexpected due to the similarity in the hydrodynamic functions for each cantilever. Furthermore, $Re$ depends only on the maximum dimension of the cantilever and not on the geometry. The ability to tailor the fluid viscosity is therefore an important design parameter. The fluid immediately surrounding the cantilever may be contained within an acoustically transparent housing and thus selected for optimum sensor response. Critical damping may be achieved with the planar cantilever using viscous fluids such as castor oil and with the cylindrical cantilever using ethylene glycol.

### B. Dependence of response on laser mode shape

According to Eq. (21), the response of the cantilever is given by the integral of the beam shape weighted by the laser intensity mode shape. The effect of the laser mode shape on the response is now investigated for the case of three mode functions given by

$$\begin{aligned} \hat{A}_1(x) &= 1, \\ \hat{A}_2(x) &= \begin{cases} 1 & 0 \le x < L/2 \\ 0 & L/2 \le x < L, \end{cases} \\ \hat{A}_3(x) &= \exp(-2q|x - L/2|). \end{aligned} \tag{22}$$

The first function corresponds to equal weighting over the beam length (i.e., a uniform mode intensity distribution), the second to unity weighting over the first half of the beam and the third corresponds to a DFB laser mode centered on the beam, where $q$ is the coupling coefficient.

The response of the cylindrical cantilever when operating in the low $Re$ regime is calculated for each of these laser mode functions and is shown in Fig. 9. The smoothest response is observed for the case of unity mode shape (solid line). If the flexural strain is integrated over half the cantilever length (dotted line), the overall response is increased by a factor ~2, however, this comes at the expense of a similar increase in the oscillation amplitude. Finally, for the case of the DFB laser mode (dashed line), the response at frequencies above the fundamental resonance is increased slightly, indicating that measuring the flexure strain close to the center of the beam yields a larger response than integrating over the total length. However, this also comes at the expense of an increase in the oscillation amplitude. The laser mode shape can therefore strongly affect the response shape and must be fully accounted for to achieve a smooth response. Similar results are obtained when the sensor operates in the moderate $Re$ regime.

### C. Comparison of planar and cylindrical cantilever

When operated in water, the cylindrical cantilever exhibits a much smoother response than the planar cantilever due to its smaller dimensions, yielding lower $Re$ of the fluid flow. However, when $Re$ is matched for each cantilever (by tailoring the fluid viscosity) the dynamic response for each geometry are very similar.

The response amplitude of the cylindrical cantilever can be dramatically increased (by a factor of 100) over that achieved by the prototype sensor by using a custom designed optical fiber incorporating a core located some distance away from the center of the optical fiber or a multi-core optical fiber.[33]

The amplitude of the response is determined by the magnitude of the driving force and the cantilever stiffness. The ratio of the driving forces for the planar and cylindrical cantilever, according to Eq. (11), is given by the ratio of their effective fluid mass, $\mu'_{\mathrm{pl}}/\mu'_{\mathrm{cyl}}$, and is typically very large ($>100$). The planar cantilever experiences a much larger driving force than the cylindrical cantilever and thus a higher response. For the simulations shown in Figs. 7 and 8 for critical damping, this leads to the planar cantilever exhibiting a

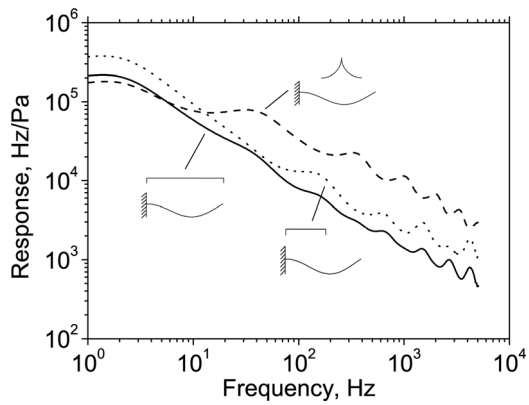


FIG. 9. Dependence of cylindrical cantilever response operating in the low $Re$ regime on laser mode shape.

response approximately 4 times higher than the cylindrical cantilever.

One characteristic of interest is the ratio of the response due to fluid motion to the response due to support motion when subjected to identical acceleration. This is given by the ratio of Eqs. (11) and (9),

$$\xi = \frac{F_{dr-FM}(\omega)}{F_{dr-SM}(\omega)} = (1 + \mu/\mu'\Gamma)^{-1} \tag{23}$$

and can be used as a figure of merit for a given cantilever geometry. The optimum value of $\xi$ is unity to avoid excess sensitivity to support motion. A value close to unity is obtained for the planar cantilever as the virtual mass of the fluid is much larger than the mass of the cantilever. A slightly less optimum value of $\xi = (1 + \rho_f/(\rho_{fl}\Gamma))^{-1} \sim 0.33$ is obtained for the cylindrical cantilever with no acrylate coating and assuming $\Gamma \sim 1$. As the fluid viscosity increases, $\xi$ for the cylindrical cantilever approaches unity.

### D. Acoustic resolution

The acoustic resolution of a cantilever type sensor can be estimated from the frequency noise of the laser. For a typical laser of the type used in the present sensor, the frequency noise is $\sim 80\,\mathrm{Hz}/\mathrm{Hz}^{1/2}$ at 100 Hz.[16] For the planar cantilever, the response at 100 Hz is measured to be ~63 100 Hz/Pa. This yields an acoustic resolution of 1.3 $\mathrm{mPa}/\mathrm{Hz}^{1/2}$, which is around a factor of 2 above the lowest sea state noise observed in the open ocean.

The simulations shown in Fig. 7 suggest a slightly higher responsivity can be obtained from the planar cantilever with a smooth frequency response. Thus, resolutions comparable to the lowest sea state noise at frequencies below 1 kHz appear attainable from the planar cantilever.

### E. Comment on the response of optical fiber to acoustically induced particle motion in water

It was shown in Fig. 6 that a small offset error in the core of conventional optical fiber yields a flexural response due to particle motion associated with a plane acoustic wave, on the order of 100 Hz/Pa. The hydrostatic pressure response of an optical fiber laser is ~330 Hz/Pa.[34] Thus, it is likely that an acoustic characterization of a supported fiber laser will be strongly influenced by the flexural response of the fiber. The same would be true if the acoustic response of the optical fiber were measured by other means such as interferometry. Furthermore, the flexural response will be larger in nonplanar fields with high levels of particle motion or for optical fiber with a larger core offset error.

These findings provide evidence that may explain the anomalously high acoustic response of submerged optical fiber lasers observed by other groups.[35,36]

## V. CONCLUSIONS

The acoustic response of planar and cylindrical fiber-optic cantilevers has been investigated both experimentally and theoretically. An analytical model of the deflections of the cantilever subject to an acoustic driving force and incorporating the effects of viscous fluid damping has been developed and applied to the case of a fiber laser cantilever. The results from an inviscid form of the analytical model are shown to be in close agreement with a 3D finite-element model based on the fluid-structure interaction up to frequencies exceeding 1 kHz. The fluid in close proximity to the cantilever is intimately coupled to the cantilever motion and the two can be thought of as acting in unison within this region. The viscid analytical model illustrates that viscous damping becomes very significant when the dimensions of the cantilever approach that of conventional optical fiber when submerged in water.

Two prototype cantilevers are characterized acoustically using a vibrating column calibrator. The response of both cantilevers is shown to yield close agreement with the predicted response from the viscid analytical model in the regime of $Re \geq 1$. In this regime the driving force is in phase with the acceleration of the cantilever and is due to the inertia of the surrounding fluid. The cylindrical cantilever yields the closest agreement due to its more uniform and defect free physical structure. The viscous fluid damping is shown to significantly reduce resonant oscillation, an effect which is observed to be strongest with the cylindrical cantilever in water due to its smaller physical size and hence lower Reynolds number of the surrounding fluid flow compared with the planar cantilever. Further reduction in $Re$ can be obtained by increasing the viscosity of the surrounding fluid. It is shown theoretically that when $Re \ll 1$, the driving force is in phase with the velocity of the surrounding fluid and as such the cantilever motion is driven by fluid viscosity. A smooth frequency response is obtained when $Re \sim 9.5 \times 10^{-4}\omega$ (~0.6 at 100 Hz) irrespective of cantilever geometry.

The response of the cantilever to support motion is also characterized and analyzed theoretically. A figure of merit is derived in terms of the ratio of the force due to fluid motion and the force due to support motion for a given cantilever geometry. Both cantilever geometries achieve a similar figure of merit. Close agreement is demonstrated between the measured response to support motion and the theoretical response.

These results will be invaluable for designing novel velocity hydrophones based around miniature cantilever configurations. Each cantilever exhibits certain benefits. For example, the cylindrical cantilever yields the smoothest response in water and is capable of dual-axis measurement of particle motion (using multicore fiber). However, the planar cantilever exhibits a higher response compared with an equivalent cylindrical cantilever with an off-axis core fiber. Thus, choice of cantilever geometry will be driven by application requirements.

Finally, we note that the response of a conventional optical fiber (i.e., with a central core) based cylindrical cantilever is close to the hydrostatic pressure response. Thus, measurement of acoustically induced strain in a submerged optical fiber will be strongly affected by the particle motion and may exhibit significant deviation from the predicted hydrostatic pressure response.

## ACKNOWLEDGMENTS

The authors would like to thank J. Bucaro (NRL), A. Tveten (NRL), J. Michalowicz (NRL), S. Foster (DSTO), and M. J. Martin (Louisiana State University) for interesting discussions during various stages of this work and J. Lou (NRL) for useful comments on the manuscript. This work was funded by the NRL 6.2 base program.

## APPENDIX A: FINITE-ELEMENT MODEL OF ACOUSTIC-STRUCTURE INTERACTION

The mechanical deformation of the planar and cylindrical cantilever subject to an acoustic wave are modeled as a coupled interaction of an acoustic wave in a fluid with a solid structure using the 3D solid, stress-strain, and acoustic modules of COMSOL MULTIPHYSICS (v3.5 a). The deformation of the cantilever with a single fixed edge, subject to a planar acoustic wave, is calculated as a function of frequency using a boundary layer mesh. The flexural strain induced in the core of the optical fiber is calculated from the deformed cantilever shape. The frequency modulation of the laser is then calculated with Eq. (21). The FE model incorporates the effect of acoustic radiation and neglects all other damping mechanisms.

## APPENDIX B: CALCULATION OF THE MECHANICAL PROPERTIES OF THE CANTILEVERS

The planar cantilever is composed of several materials (aluminum, acrylate, and silica glass) and as such has to be treated as a composite structure. However, several simplifications can be made due to the uniformity of the cantilever along its length. In this case, the elastic properties of the composite structure can be determined by (a) deriving the equivalent cross-section area, (b) determining the position of the neutral surface, and (c) using the parallel axis theorem to determine the second moment of area.

This procedure, applied to an identical cross-sectional structure, is described in Sec. III B of Ref. 37 and is used in the present model.

## APPENDIX C: ACOUSTIC CHARACTERIZATION WITH A VIBRATING COLUMN

Characterization of the acoustic response of the cantilever in a fluid is achieved using a technique known as the vibrating water column method described in Ref. 38. This method produces a well defined and highly uniform acceleration field in a single plane and is thus highly suited to characterizing acoustic vector sensors. Illustrated in Fig. 10, the cantilever is placed in a rigid walled container of water, which is excited on a vibration table. The vibration of the column induces an acoustic field in the water column. The acceleration of the fluid as a function of depth, $\ddot{u}(h)$, is given by

$$\frac{\ddot{u}(h)}{\ddot{u}_1} = \frac{\cos(\omega h/c_c)}{\cos(\omega d/c_c)}, \tag{C1}$$

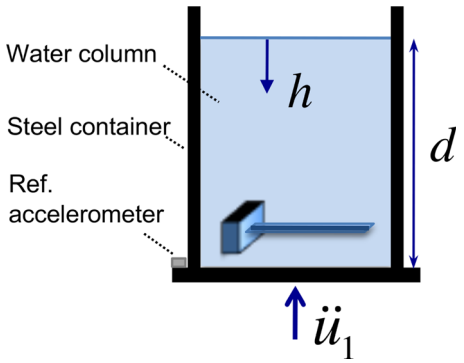


FIG. 10. (Color online) Vibrating column calibrator.

where $\ddot{u}_1$ is the acceleration applied at the base of the column, $h$ is the depth, $d$ is the height of the water column, and $c_c$ is the sound speed in the column. For an infinitely rigid column $c_c$ is equal to the bulk sound speed of water. The response of the cantilever is measured relative to the response of the accelerometer attached to the base. At frequencies less than 500 Hz and close to the bottom of the column, $\ddot{u}(h) \sim \ddot{u}_1$.

This calibration technique has other useful characteristics. The water-air interface acts as a pressure release surface at which the pressure is zero. Any residual response to acoustic pressure can be determined by varying the depth of the cantilever and taking into account any variation in $\ddot{u}(h)$. The local pressure can be obtained from the specific acoustic impedance of the column given by

$$\frac{p(h)}{\dot{u}(h)} = i\rho c_c \tan\left(\frac{\omega h}{c_c}\right), \tag{C2}$$

where $\dot{u} = \ddot{u}/(i\omega)$. The response of the cantilever in terms of the acoustic pressure in a free-field, $p_{ff}$, is determined from

$$p_{ff} = \ddot{u}\frac{\rho_{fl} c_{fl}}{i\omega}. \tag{C3}$$

This represents a *standard* field for comparing acoustic sensors

[1]G. D'Spain, J. Luby, G. Wilson, and R. Gramann, "Vector sensors and vector sensor line arrays: Comments on optimal array gain and detection," J. Acoust. Soc. Am. **120**(1), 171–185 (2006).
[2]A. Nehorai and E. Paldi, "Acoustic vector-sensor array processing," IEEE Trans. Signal Process. **42(9)**, 2481–2491 (1994).
[3]T. Gabrielson, D. Gardner, and S. Garrett, "A simple neutrally buoyant sensor for direct measurement of particle velocity and intensity in water," J. Acoust. Soc. Am. **97**(4), 2227–2237 (1996).
[4]B. Abraham, "Low-cost dipole hydrophone for use in towed arrays," AIP Conf. Proc. **368**, 189–201 (1996).
[5]J. Shipps and K. Deng, "A miniature vector sensor for line array applications," in *OCEANS 2003 Proceedings* (2003), Vol. 5, pp. 2367–2369.
[6]H. De Bree, P. Leussink, T. Korthorst, H. Jansen, T. S. J. Lammerink, and M. Elwenspoek, "The $\mu$-flown: A novel device for measuring acoustic flows," Sens. Actuators, A **54**, 552–557 (1996).
[7]J. Butler, D. M. S. C. Butler, and G. Cavanagh, "Metallic glass velocity sensor," AIP Conf. Proc. **368**, 101–133 (1996).
[8]G. Cranch and P. Nash, "High responsivity fiber-optic flexural disk accelerometers," J. Lightwave Technol. **19**(7), 1233–1243 (2000).

[9]S. T. Vohra, B. Danver, A. Tveten, and A. Dandridge, "Fiber optic interferometric accelerometers," AIP Conf. Proc. **368**, 285–293 (1996).
[10]P. Jackson, S. Foster, and S. Goodman, "A fiber laser acoustic vector sensor," Proc. SPIE **7503**, 750329 (2009).
[11]A. M. Yurek, B. A. Danver, A. B. Tveten, and A. Dandridge, "Fiber optic gradient hydrophones," Proc. SPIE **2360**, 364–367 (1994).
[12]G. Cranch, G. Miller, and C. Kirkendall, "Low frequency acoustic response of a planar fiber laser cantilever in a fluid," Proc. SPIE **7753**, 775334 (2011).
[13]J. Cole, R. Johnson, and P. Bhuta, "Fiber-optic detection of sound," J. Acoust. Soc. Am. **62**(5), 1136–1138 (1977).
[14]J. Bucaro and T. Hickman, "Measurement of sensitivity of optical fibers for acoustic detection," Appl. Opt. **18**(6), 938–940 (1977).
[15]J. Bucaro, N. Lagakos, J. Cole, and T. Giallorenzi, "Fiber-optic acoustic transduction," Phys. Acoust. **XVI**, 385–457 (1982).
[16]G. Cranch, G. Flockhart, and C. Kirkendall, "Distributed feedback fiber laser strain sensors," IEEE Sens. J. **8**(7), 1161–1172 (2008).
[17]L. Yuan, J. Yang, and Z. Liu, "A compact fiber-optic flow velocity sensor based on a twin-core fiber michelson interferometer," IEEE Sens. J. **8**(7), 1114–1117 (2008).
[18]M. Josserand and C. Maerfeld, "Pvf2 velocity hydrophones," J. Acoust. Soc. Am. **78**(3), 861–867 (1970).
[19]J. Sader, "Frequency response of cantilever beams immersed in viscous fluids with applications to the atomic force microscope," J. Appl. Phys. **84**(1), 64–76 (1998).
[20]U. Lindholm, D. Kana, W. Chu, and H. Abramson, "Elasic vibration characteristics of cantilever plates in water," J. Ship Res. **9**(11), 11–22 (1965).
[21]L. Landweber, "Vibration of a flexible cylinder in a fluid," J. Ship Res. **11**(143), 143–150 (1967).
[22]A. Jones, "Vibration of beams immersed in a liquid," Exp. Mech **10**(84), 84–88 (1970).
[23]J. Bailey and F. Fahy, "Radiation and response of cylindrical beams excited by sound," J. Eng. Ind. **9**(11), 11–22 (1972).
[24]D. G. Crighton, "Resonant oscillations of fluid-loaded struts," J. Sound Vib. **87**(3), 429–437 (1983).
[25]J. Achenbach and J. Qu, "Resonant vibrations of a submerged beam," J. Sound Vib. **105**(2), 185–198 (1986).
[26]J. Chon, P. Mulvaney, and J. Sader, "Experimental validation of theoretical models for the frequency response of atomic force microscope caniltever beams immersed in fluids," J. Appl. Phys. **87**(8), 3978–3988 (2000).
[27]L. Rosenhead, *Laminar Boundary Layers* (Oxford University Press, Oxford, 1963), Chap. VII.
[28]X. Xu and A. Raman, "Comparative dynamics of magnetically, acoustically, and Brownian motion driven microcantilevers in liquids," J. Appl. Phys. **102**, 1–8 (2007).
[29]L. Kinsler, A. Frey, A. Coppens, and J. Saunders, *Fundamentals of Acoustics*, 3rd ed. (Wiley, New York, 1982), Sec. 5.4.
[30]W. Chu, "Vibration of fully submerged cantilever plates in water," Southwest Research Institute Technical Report No. 2 DTMB, Contract Nobs-86396 (X) (April, 1963).
[31]H. Lin and S. Chen, "Acoustically induced vibration of circular cylindrical rods," J. Sound Vib. **51**(1), 89–96 (1977).
[32]S. Foster, "Spatial mode structure of the distributed feedback fiber laser," IEEE J. Quantum Electron. **40**, 884–892 (2004).
[33]G. Flockhart, W. MacPherson, J. Barton, J. Jones, L. Zhang, and I. Bennion, "Two-axis bend measurement with Bragg gratings in multicore optical fiber," Opt. Lett. **28**(6), 387–389 (2003).
[34]Static pressure response of fiber laser measured in our laboratory by recording the laser frequency shift as a function of the hydrostatic pressure.
[35]D. Hill, P. Nash, D. Webb, S. F. O'Neill, L. Bennion, and L. Zhang, "A fiber laser hydrophone array," Proc. SPIE **3860**, 55–65 (1999).
[36]A. Tikhomirov, S. Foster, M. Milnes, and G. Hardy, "Acoustic and vibrational response of a DFB fibre laser hydrophone," COIN/ACOFT Melborne (2003), p. 440–443.
[37]G. Cranch, G. Flockhart, and C. Kirkendall, "High-resolution distributed-feedback fiber laser dc magnetometer based on the Lorentzian force," Meas. Sci. Technol. **20**, 034023 (2009).
[38]F. Schloss and M. Strasberg, "Hydrophone calibration in vibrating column of liquid," J. Acoust. Soc. Am. **34**(7), 958–960 (1962).